

Non-equilibrium dynamics of dense gas under tight confinement

Lei Wu^{1,†}, Haihu Liu², Jason M. Reese³ and Yonghao Zhang¹

¹James Weir Fluids Laboratory, Department of Mechanical and Aerospace Engineering, University of Strathclyde, Glasgow G1 1XJ, UK

²School of Energy and Power Engineering, Xi'an Jiaotong University, 28 West Xianning Road, Xi'an 710049, China

³School of Engineering, University of Edinburgh, Edinburgh EH9 3FB, UK

(Received 6 December 2015; revised 25 January 2016; accepted 27 February 2016)

The force-driven Poiseuille flow of dense gases between two parallel plates is investigated through the numerical solution of the generalized Enskog equation for two-dimensional hard discs. We focus on the competing effects of the mean free path λ , the channel width L and the disc diameter σ . For elastic collisions between hard discs, the normalized mass flow rate in the hydrodynamic limit increases with L/σ for a fixed Knudsen number (defined as $Kn = \lambda/L$), but is always smaller than that predicted by the Boltzmann equation. Also, for a fixed L/σ , the mass flow rate in the hydrodynamic flow regime is not a monotonically decreasing function of Kn but has a maximum when the solid fraction is approximately 0.3. Under ultra-tight confinement, the famous Knudsen minimum disappears, and the mass flow rate increases with Kn , and is larger than that predicted by the Boltzmann equation in the free-molecular flow regime; for a fixed Kn , the smaller L/σ is, the larger the mass flow rate. In the transitional flow regime, however, the variation of the mass flow rate with L/σ is not monotonic for a fixed Kn : the minimum mass flow rate occurs at $L/\sigma \approx 2-3$. For inelastic collisions, the energy dissipation between the hard discs always enhances the mass flow rate. Anomalous slip velocity is also found, which decreases with increasing Knudsen number. The mechanism for these exotic behaviours is analysed.

Key words: granular media, micro-/nano-fluid dynamics, non-continuum effects

1. Introduction

Gas transportation along micro/nanoscale channels exhibits unusual behaviour that cannot be captured by conventional computational fluid dynamics (Karniadakis, Beskok & Aluru 2005; Holt *et al.* 2006). One well-known phenomenon is the Knudsen paradox (Knudsen 1909): when a constant pressure difference drives flow along a narrow channel, the mass flow rate (MFR) displays a characteristic minimum as the inlet pressure is reduced, although the conventional Navier–Stokes equations

† Email address for correspondence: lei.wu.100@strath.ac.uk

simply predict a monotonic decreasing MFR. As the ratio of the gas molecular mean free path to the channel width (the Knudsen number, Kn) becomes appreciable in narrow channels, the Boltzmann equation is commonly used to describe the collective motion of a dilute gas from the hydrodynamic to the free-molecular flow regimes (Chapman & Cowling 1970). From numerical analysis of the Boltzmann equation (Ohwada, Sone & Aoki 1989a), the Knudsen minimum may be understood as a consequence of the competition between the gas velocity slip at the channel wall and the effective shear viscosity, which both increase with the Knudsen number: while larger velocity slip increases the MFR, higher effective viscosity decreases the MFR by making the velocity profile flatter. The minimum MFR occurs at $Kn \sim 1$.

Poiseuille flow with non-negligible Knudsen numbers has received much attention in recent years, due to the development of micro/nano-electromechanical systems (Karniadakis *et al.* 2005) and the shale gas revolution (Wang *et al.* 2014). The MFR obtained from the Boltzmann equation is a key parameter in the generalized Reynolds equation to describe gas-film lubrication problems such as the gas slide bearing (Fukui & Kaneko 1987, 1990; Cercignani, Lampis & Lorenzani 2007), as well as in the upscaling methods used to predict the gas permeability of ultra-tight shale strata (Darabi *et al.* 2012; Mehmani, Prodanović & Javadpour 2013; Lunati & Lee 2014; Ma *et al.* 2014).

While the Boltzmann equation is a fundamental model for gas dynamics at low pressures, its applicability to a typical shale gas production scenario, with gas pressures of the order of 10^6 – 10^7 Pa, is problematic (Ma *et al.* 2014). This is because the Boltzmann equation is derived under the assumption that the mean free path is much larger than the molecular dimension, but this is not the case for large gas pressures. Instead, the Enskog equation, which takes into account the finite size of gas molecules and non-local collisions, has been developed for dense gases (Chapman & Cowling 1970). Although the original equation is for hard-sphere molecules, long-range intermolecular attractive forces can be included through a mean-field theory (Grmela 1971; Karkheck & Stell 1981), so that the van der Waals' equation of state can be recovered. The extended Enskog equation has successfully described gas–liquid phase transitions, net condensation/evaporation and liquid menisci between two solid surfaces (Frezzotti, Gibelli & Lorenzani 2005; Kon, Kobayashi & Watanabe 2014; Barbante, Frezzotti & Gibelli 2015), with numerical results in good agreement with molecular dynamics simulations (Frezzotti 1998; Frezzotti *et al.* 2005).

For the Poiseuille flow of dense gases, there are three characteristic length scales: the mean free path, the channel width and the molecular diameter. The purpose of this paper is to investigate the influence of these competing length scales on the MFR in force-driven flow, through numerical solution of the Enskog equation. Our investigation is not, however, limited to elastic collisions between gas molecules, but is extended to dissipative collisions in dense granular gases, i.e. agitated ensembles of macroscopic grains modelled as inelastic hard discs or spheres (Brilliantov & Pöschel 2004; Aranson & Tsimring 2006). For simplicity, we consider the dense flow of hard discs in this paper, which is modelled by the generalized Enskog equation in §2. In §3, numerical results of the Enskog equation are presented, and analytical models are proposed to explain the unexpected behaviour of the MFR and the slip velocity. Finally, we draw conclusions in §4.

2. The generalized Enskog equation for dense granular gases

Consider a granular gas composed of smooth hard discs of diameter σ and mass m , subject to an external acceleration a in the x direction, and confined between two infinite parallel plates of temperature T_w at $y = \pm(L + \sigma)/2$. Since the hard discs

cannot fully occupy the region less than half a disc diameter away from a plate, L is regarded as the effective channel width. The impact of two hard discs conserves mass and momentum but not kinetic energy. Suppose \mathbf{v} and \mathbf{v}_* are, respectively, the pre-collision velocities of a first and a second hard disc. The corresponding post-collision velocities \mathbf{v}' and \mathbf{v}'_* are given by

$$\mathbf{v}' = \mathbf{v} - \frac{(1 + \alpha)}{2}(\mathbf{u} \cdot \mathbf{k})\mathbf{k}, \quad \mathbf{v}'_* = \mathbf{v}_* + \frac{(1 + \alpha)}{2}(\mathbf{u} \cdot \mathbf{k})\mathbf{k}, \quad (2.1a,b)$$

where $\mathbf{u} = \mathbf{v} - \mathbf{v}_*$ is the relative collision velocity, \mathbf{k} is the unit vector from the centre of the first disc to the centre of the second at the time of their impact, and α is the restitution coefficient characterizing the loss of the normal relative velocity, i.e. $\mathbf{k} \cdot (\mathbf{v}' - \mathbf{v}'_*) = -\alpha\mathbf{k} \cdot \mathbf{u}$. The collision is elastic when $\alpha = 1$ and inelastic when $0 \leq \alpha < 1$.

When the disc number density n is small, so that the mean free path ($1/2\sqrt{2}n\sigma\chi(n)$, where χ is the pair correlation function defined below) is much larger than the disc diameter, the dynamics of the dilute granular gas is modelled by the generalized Boltzmann equation (Goldstein & Shapiro 1995). However, as the number density increases, the mean free path could become much smaller than the disc diameter, in which case the localized collision assumption in the Boltzmann equation is invalid and the finite area of the hard discs becomes important. The generalized Enskog equation (Esteban & Perthame 1991; Brey, Dufty & Santos 1997; Bobylev, Carrillo & Gamba 2000) describes the flow of dense granular gases, where the velocity distribution function $f(y, \mathbf{v})$, which is a function of the hard-disc velocity $\mathbf{v} = (v_x, v_y)$ and spatial location y , is governed by

$$v_y \frac{\partial f}{\partial y} + F \frac{\partial f}{\partial v_x} = n_0 \sigma L \iint (\mathbf{k} \cdot \mathbf{u}) \left[\frac{J}{\alpha} g(y, \mathbf{k}, \tilde{\mathbf{v}}_*) f(y, \tilde{\mathbf{v}}) - g(y, -\mathbf{k}, \mathbf{v}_*) f \right] d\mathbf{v}_* d\mathbf{k}, \quad (2.2)$$

in which time is omitted because we are only interested in the steady-state profiles. Here $F = maL/2k_B T_w$ is the dimensionless acceleration, k_B is the Boltzmann constant, n_0 is the average number density, and J is the Jacobian of the transformation from $(\tilde{\mathbf{v}}, \tilde{\mathbf{v}}_*)$ into $(\mathbf{v}, \mathbf{v}_*)$, where $\tilde{\mathbf{v}}$ and $\tilde{\mathbf{v}}_*$ are the pre-collision velocities producing post-collision velocities \mathbf{v} and \mathbf{v}_* . For hard-disc gases, collisions are instantaneous, and multiple encounters can be neglected (Chapman & Cowling 1970). The binary collision is non-local, as the distance between the mass centres of the two colliding hard discs is the hard-disc diameter. Such non-local collisions are characterized by the product of the distribution function and a pair correlation function at different locations, i.e.

$$g(y, \mathbf{k}, \mathbf{v}) = f \left(y + \frac{\sigma k_y}{L}, \mathbf{v} \right) \chi \left[n \left(y + \frac{\sigma k_y}{2L} \right) \right]. \quad (2.3)$$

Here k_y is the projection of \mathbf{k} in the y direction, and the pair correlation function χ is given by (Sanchez 1994)

$$\chi(n) = \frac{1}{2} \frac{2 - \eta(n)}{[1 - \eta(n)]^2}, \quad (2.4)$$

which, compared to other expressions (Henderson 1975; Baus & Colot 1987), is accurate for the solid fraction $\eta = \pi\sigma^2 n n_0/4$ up to the square-packing density $\eta = \pi/4$.

Note that in writing (2.2) the location y is normalized by the effective channel width L , the number density n is normalized by n_0 , velocity is normalized by the

most probable speed $v_m = \sqrt{2k_B T_w/m}$, temperature T is normalized by T_w , and the velocity distribution function f is normalized by n_0/v_m^2 . When the velocity distribution function is known, the normalized number density, flow velocity and temperature are given as follows: $n(y) = \int f(y, \mathbf{v}) d\mathbf{v}$, $U_x(y) = \int f(y, \mathbf{v}) v_x d\mathbf{v}/n(y)$ and $T(y) = \int f(y, \mathbf{v}) [(v_x - U_x)^2 + v_y^2] d\mathbf{v}/n(y)$. The MFR, which is normalized by $n_0 m L^2 a/v_m$, is defined as

$$\mathcal{M} = \int_{-1/2}^{1/2} n(y) U_x(y) dy / F \equiv \int_{-1/2}^{1/2} n(y) V_x(y) dy, \quad (2.5)$$

where the integration range of the normalized y is from $-1/2$ to $1/2$ because the centres of the hard discs are confined to this region such that macroscopic quantities outside of this region of y vanish.

3. Numerical and analytical results

We solve the generalized Enskog equation (2.2) by using the fast spectral method (Wu, Zhang & Reese 2015) under the constraint $\int_{-1/2}^{1/2} n(y) dy = 1$, for various values of L/σ and the global Knudsen number

$$Kn = \frac{\lambda_{HS}}{L} = \frac{1}{2\sqrt{2}n_0\sigma\chi(1)L}, \quad (3.1)$$

together with the diffuse boundary condition (Galvin, Hrenya & Wildman 2007)

$$f(y = \pm 1/2, \mathbf{v})|_{v_y \leq 0} = \frac{n_w}{\pi} \exp(-v^2), \quad (3.2)$$

where $n_w = \pm 2\sqrt{\pi} \int_{v_y \geq 0} v_2 f(y = \pm 1/2, \mathbf{v}) d\mathbf{v}$. Note that the collisions in the Boltzmann equation are local, and the Boltzmann equation is recovered if we choose $g(y, \mathbf{k}, \mathbf{v})$ in (2.3) as $g(y, \mathbf{k}, \mathbf{v}) = f(y, \mathbf{v})$ and $Kn = 1/2\sqrt{2}n_0\sigma L$.

3.1. Elastic collisions: $\alpha = 1$

We consider the case where the external acceleration is very small ($F = 0.0001$). The Enskog equation (2.2) is solved from $\eta \approx 0$, until the maximum solid fraction reaches the square-packing limit. The MFR is shown in figure 1 as a function of the Knudsen number at several values of L/σ . For the Boltzmann equation, the Knudsen minimum is clearly seen at $Kn \sim 1$, and when $Kn < 1$ (> 1), the MFR decreases (increases) monotonically with Kn . For the Enskog equation, the MFR is significantly influenced by the tightness of the wall confinement. When the channel width is large ($L/\sigma \geq 50$), the MFR at $Kn \geq 1$ is the same as that from the Boltzmann equation, while the MFR for $Kn < 1$ is smaller than that from the Boltzmann equation, and the difference increases as Kn decreases. As L/σ decreases, the MFR becomes smaller, and the difference from the Boltzmann result gradually extends to large Knudsen numbers. For $L/\sigma > 5$, the MFR is not a monotonically decreasing function of Kn in the slip flow regime ($Kn < 0.1$). Instead, there exists a specific value of Kn at which the MFR is locally maximum, i.e. $Kn = 0.02$ when $L/\sigma = 30$, $Kn = 0.05$ when $L/\sigma = 15$, and $Kn = 0.08$ when $L/\sigma = 10$. For $L/\sigma \leq 5$, the Knudsen minimum actually disappears, and the MFR only increases with the Knudsen number. Also, in the free-molecular regime ($Kn > 10$), the MFR is larger than the Boltzmann prediction.

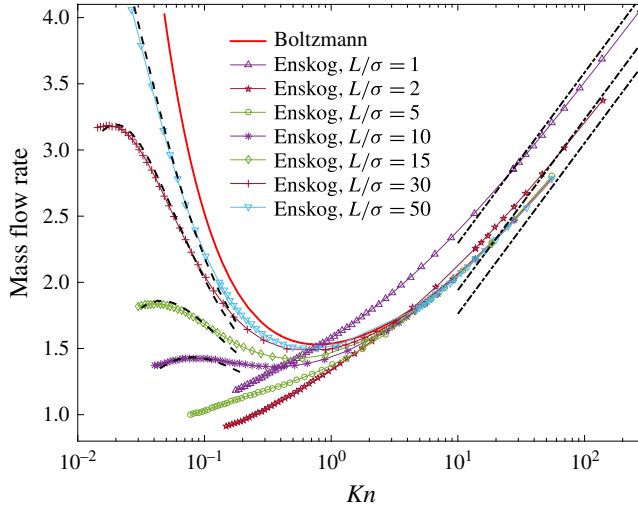


FIGURE 1. (Colour online) The mass flow rate as a function of the Knudsen number, for various values of L/σ , when the collision between the hard discs is elastic. Dashed lines: numerical results of the Navier–Stokes equation (3.8) with the first-order velocity slip boundary condition (3.10). Dash-dotted lines: the asymptotic analytical solutions (3.5) as $Kn \rightarrow \infty$; from top to bottom, $L/\sigma = 1, 2$ and 10 .

We now examine the influence of the channel width on the MFR in the free-molecular regime. This regime occurs at small solid fractions. As with the Boltzmann equation, the normalized number density is unitary across the channel; however, the non-local collision in the Enskog equation makes the collision frequency spatially varying, which consequently affects the MFR. For small external accelerations, the distribution function can be linearized around the global equilibrium distribution function $f_{eq}(\mathbf{v}) = \exp(-\mathbf{v}^2)/\pi$ as $f(y, \mathbf{v}) = f_{eq}(\mathbf{v})[1 + h(y, \mathbf{v})]$. The equilibrium collision frequency reads (as the pair correlation function is approximately 1)

$$v(y, \mathbf{v}) = \iint (\mathbf{k} \cdot \mathbf{u}) f_{eq}(\mathbf{v}_*) H\left(y - \frac{\sigma k_y}{L}\right) d\mathbf{v}_* d\mathbf{k}, \tag{3.3}$$

where $H(y)$ is unitary for $|y| \leq 1/2$ and zero otherwise. The mean collision frequency $\bar{v}(y) = \int f_{eq}(\mathbf{v}) v(y, \mathbf{v}) d\mathbf{v}$ is plotted in figure 2 for various values of L/σ . For the Boltzmann equation with localized collisions, the mean collision frequency is a straight line with the value 2.507. For the Enskog equation, however, the non-local collision reduces the collision frequency in the region within one hard-disc diameter from the wall. For instance, the mean collision frequency at the wall for $L/\sigma \geq 1$ is half that of the Boltzmann equation because half of the collision is shielded by the wall.

When $Kn \rightarrow \infty$, the collision term $J\alpha^{-1}g(y, \mathbf{k}, \tilde{\mathbf{v}}_*)f(y, \tilde{\mathbf{v}})$ in (2.2) can be neglected (Cercignani 1963; Takata & Funagane 2011). After linearization, the Enskog equation is approximated by the following equation for the deviational distribution function $h(y, \mathbf{v})$:

$$v_y \frac{\partial h}{\partial y} - 2Fv_x = -n_0\sigma Lv \left(y, \mathbf{v}, \frac{L}{\sigma}\right) h \sim -n_0\sigma L\bar{v} \left(\frac{L}{\sigma}\right) h = -\frac{1}{2\sqrt{2}Kn} \bar{v} \left(\frac{L}{\sigma}\right) h. \tag{3.4}$$

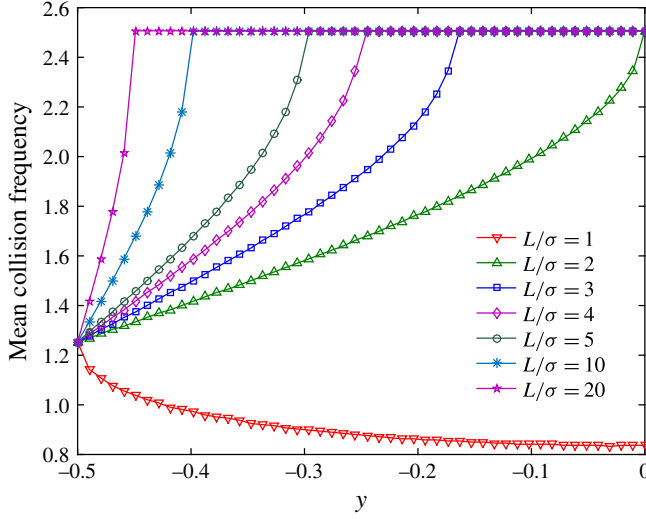


FIGURE 2. (Colour online) The mean collision frequency $\tilde{v}(y, L/\sigma) = \int f_{eq}(\mathbf{v})v(y, \mathbf{v}) d\mathbf{v}$ for various values of L/σ , with $n_0 \rightarrow 0$. For symmetry, only half the spatial domain is plotted. Values of the spatially averaged mean collision frequency $\bar{v} = \int \tilde{v}(y) dy$ are 0.911, 1.709, 1.974, 2.107, 2.187, 2.347 and 2.428, when $L/\sigma = 1, 2, 3, 4, 5, 10$ and 20 , respectively.

Here $\bar{v} = \int \tilde{v}(y) dy$ is the spatial average of the mean collision frequency, which decreases with L/σ (see the caption of figure 2). With the diffuse boundary condition $h(y = \pm 1/2, v_y \leq 0) = 0$, the final expression for the MFR at the asymptotic limit $Kn \rightarrow \infty$ is

$$\mathcal{M} \left(Kn, \frac{L}{\sigma} \right) = \frac{1}{\sqrt{\pi}} \left[\ln Kn + \ln(2\sqrt{2}) - \ln \bar{v} \left(\frac{L}{\sigma} \right) \right] + \frac{3(1 - \gamma)}{2\sqrt{\pi}}, \quad (3.5)$$

where $\gamma \approx 0.577216$ is the Euler constant. This analytical solution is plotted in figure 1 as dash-dotted lines, where good agreement with fast spectral solutions of the Enskog equation (Wu *et al.* 2015) can be seen when $Kn > 30$.

We turn to the flow in the hydrodynamic slip regime. The solid fraction η is high, and the number density obtained from the Enskog equation is not uniform across the channel (unlike for the Boltzmann equation, where the normalized number density is unitary when the external acceleration is small). Substituting the local equilibrium distribution function $f(y, \mathbf{v}) = n(y)f_{eq}(\mathbf{v})$ into (2.2), we obtain the following equation for the density variation:

$$\frac{dn}{dy} = \frac{n}{\sqrt{2}Kn} \int_{-\pi/2}^{\pi/2} H \left(y - \frac{\sigma \sin \theta}{L} \right) n \left(y - \frac{\sigma \sin \theta}{L} \right) \chi \left[n \left(y - \frac{\sigma \sin \theta}{2L} \right) \right] \sin \theta d\theta, \quad (3.6)$$

which is numerically solved by an iterative method (Frezzotti 1997) under the constraint $\int_{-1/2}^{1/2} n(y) dy = 1$. Typical equilibrium density profiles are shown in figure 3. Near the wall, the density decreases monotonically under ultra-tight confinement (i.e. $L/\sigma = 2$), but oscillates in the region within one to two hard-disc diameters from the wall when L/σ is large (i.e. $L/\sigma = 10$). Generally speaking, the larger the solid fraction, the larger the local disc density near the wall.

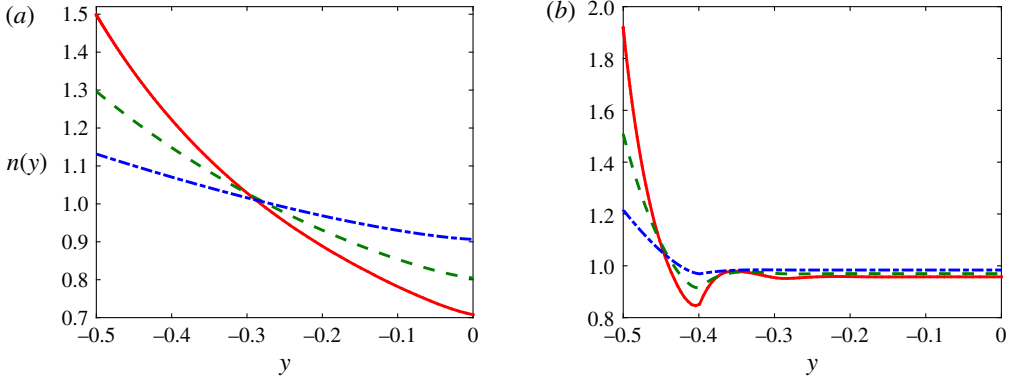


FIGURE 3. (Colour online) Normalized density profiles of the dense gas under tight confinements (a) $L/\sigma = 2$ and (b) $L/\sigma = 10$. The solid fractions, based on the average number density n_0 , are $\eta = 0.3, 0.2$ and 0.1 for the solid, dashed and dash-dotted lines, respectively.

The density variation across the channel affects the gas slip velocity along the wall and the curvature of the velocity profile. To obtain quantitative estimates, we consider the Navier–Stokes equation with the first-order velocity slip boundary condition. Since the shear viscosity of the dense hard-disc system is (Garcia-Rojo, Luding & Brey 2006)

$$\mu = \frac{1}{2\sigma} \sqrt{\frac{mk_B T}{\pi}} \left[\frac{1}{\chi(1)} + 2\eta(1) + \left(1 + \frac{8}{\pi}\right) \chi(1)\eta(1)^2 \right], \quad (3.7)$$

the Navier–Stokes equation can be written as

$$\frac{\partial}{\partial y} \left(Kn_e \frac{\partial V_x}{\partial y} \right) = -\sqrt{\pi} n(y), \quad (3.8)$$

where the effective Knudsen number is

$$Kn_e = Kn \frac{\chi(1)}{\chi(n)} \left\{ 1 + 2b + \left(1 + \frac{8}{\pi}\right) b^2 \right\}, \quad (3.9)$$

and $b = \chi(n)\eta(n)$. To exclude the effect of the wall on the shear viscosity, we choose $b(y)$ for $y < -0.5 + \sigma/L$ or $y > 0.5 - \sigma/L$ to be $b(y) = 0$.

The first-order slip boundary condition at $y = \pm 1/2$ can be written as

$$V_x(y) = -C \frac{Kn_e}{n(y)} \frac{\partial V_x}{\partial y} = C \frac{\sqrt{\pi}}{2n(y)}, \quad (3.10)$$

where the constant is set to be $C = 1.11$ from the Boltzmann equation for hard-sphere molecules (Ohwada, Sone & Aoki 1989b; Hadjiconstantinou 2003). Note that the second equation in (3.10) is derived from (3.8) using the symmetry condition $\partial V_x / \partial y = 0$ at $y = 0$ and the normalization condition $\int_{-1/2}^{1/2} n(y) dy = 1$.

Although the slip velocity from the Enskog equation is smaller than that from the Boltzmann equation, the ‘momentum slip’, i.e. $V_x(\pm 0.5)n(\pm 0.5)$, is the same for both equations. Therefore, the MFR predicted by the Enskog equation is smaller than that from the Boltzmann equation in the hydrodynamic flow regime because $Kn_e > Kn$,

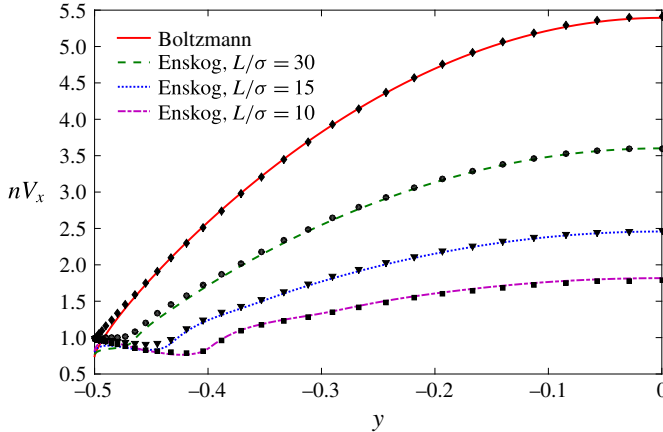


FIGURE 4. (Colour online) Typical momentum profiles of the dense gas in the slip flow regime ($Kn = 0.05$). Solid symbols represent numerical solutions of the Navier–Stokes equation (3.8). The momentum profile from the Enskog equation is not a monotonically increasing function of y from the wall to the channel centre, because of the non-monotonic density variations.

which makes the velocity profile by the Enskog equation much flatter than that by the Boltzmann equation. At the same Kn , as a smaller L/σ has a larger solid fraction η , and larger η leads to larger Kn_e/Kn , the MFR decreases with the ratio L/σ , as can be seen in figure 1. Typical momentum profiles in the hydrodynamic flow regime are shown in figure 4, where good agreement between the fast spectral solutions of the Enskog equation (Wu *et al.* 2015) and the solutions of the Navier–Stokes equation can be found. We have also plotted the MFR from the Navier–Stokes equation in figure 1, showing that (3.8) is a good predictor of the MFR when $Kn < 0.1$.

If L/σ is fixed, the effective Knudsen number decreases as the solid fraction η increases, hence the MFR should increase with the solid fraction and decrease with the global Knudsen number. From figure 1 we see that this is true in most cases. However, there is a critical point after which the MFR decreases although η increases (and the MFR decreases with decreasing Kn): for instance, see the curve of $L/\sigma = 10$ for $Kn < 0.08$ in figure 1, although the variation is quite small. This is because, at large η , there is a significant dip in the number density at $y \approx \pm(0.5 - \sigma/L)$, and this density dip may reduce the overall MFR. An illustrative example is shown in figure 5.

Finally, we consider the transitional flow regime, which usually has a global Knudsen number ranging from approximately 0.1 to 10. Neither the hydrodynamic nor the free-molecular theories can explain the flow behaviour. Even for the Boltzmann equation, the regularized 26-moment equation of Gu & Emerson (2009) can only give accurate results up to $Kn \sim 1$. Since the MFR increases with decreasing L/σ in the free-molecular flow regime, and the MFR increases with L/σ in the hydrodynamic regime, in the transitional regime there should exist a specific value of L/σ at which the MFR is minimum for a particular Kn . Numerical results confirm that this minimum MFR occurs at $L/\sigma \approx 2\text{--}3$ in the transitional regime (see figure 6).

3.2. Inelastic collisions: $0 \leq \alpha < 1$

In the dilute limit $\eta \rightarrow 0$, the behaviour of the MFR was studied by Alam, Mahajan & Shivanna (2015) using molecular dynamics simulations, and an anomalous velocity

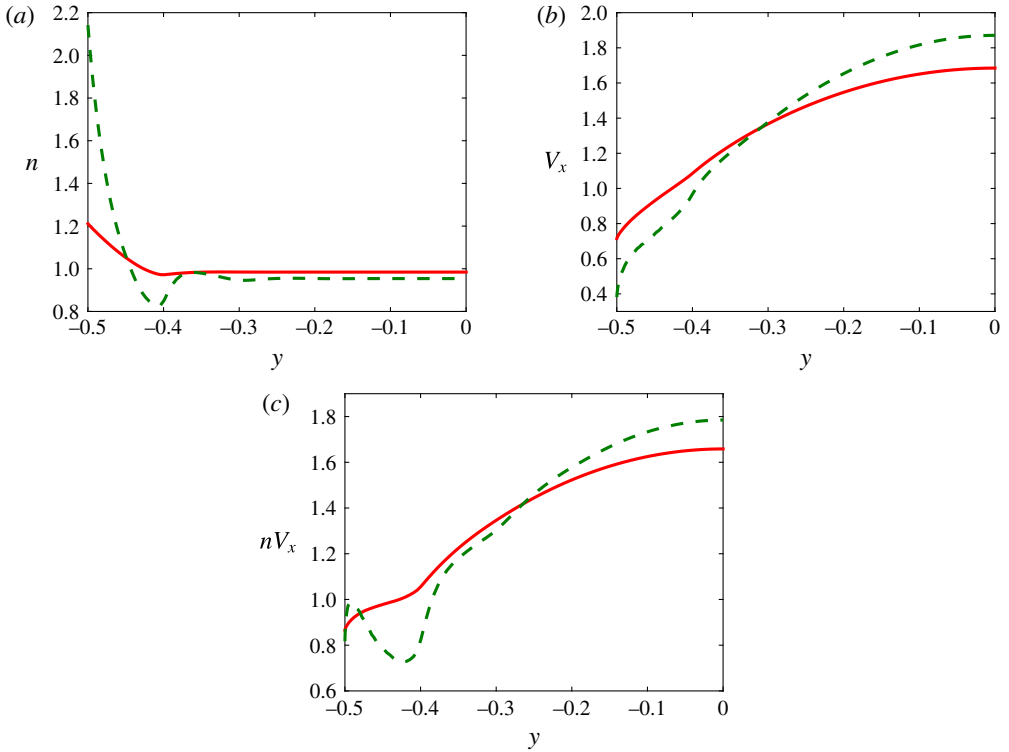


FIGURE 5. (Colour online) Macroscopic profiles of the dense gas for $Kn=0.237$ ($\eta=0.10$, solid lines) and $Kn=0.041$ ($\eta=0.35$, dashed lines) when $L/\sigma = 10$. Although a larger value of η means the momentum in the channel centre is larger, the significant dip in the density for larger η reduces the local MFR, so that the two curves have the same overall MFR.

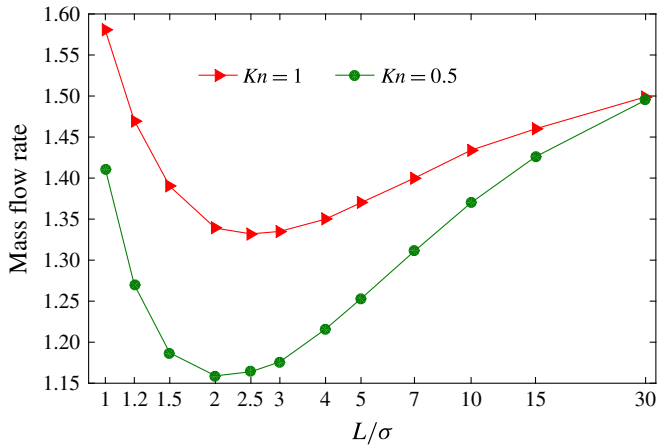


FIGURE 6. (Colour online) MFR varying with L/σ for the dense gas when $Kn=0.5$ and $Kn=1$.

slip (i.e. the slip velocity decreases as Kn increases) was observed. Here we investigate the origin of this anomalous velocity slip, and calculate the MFR of dilute-to-dense granular gases.

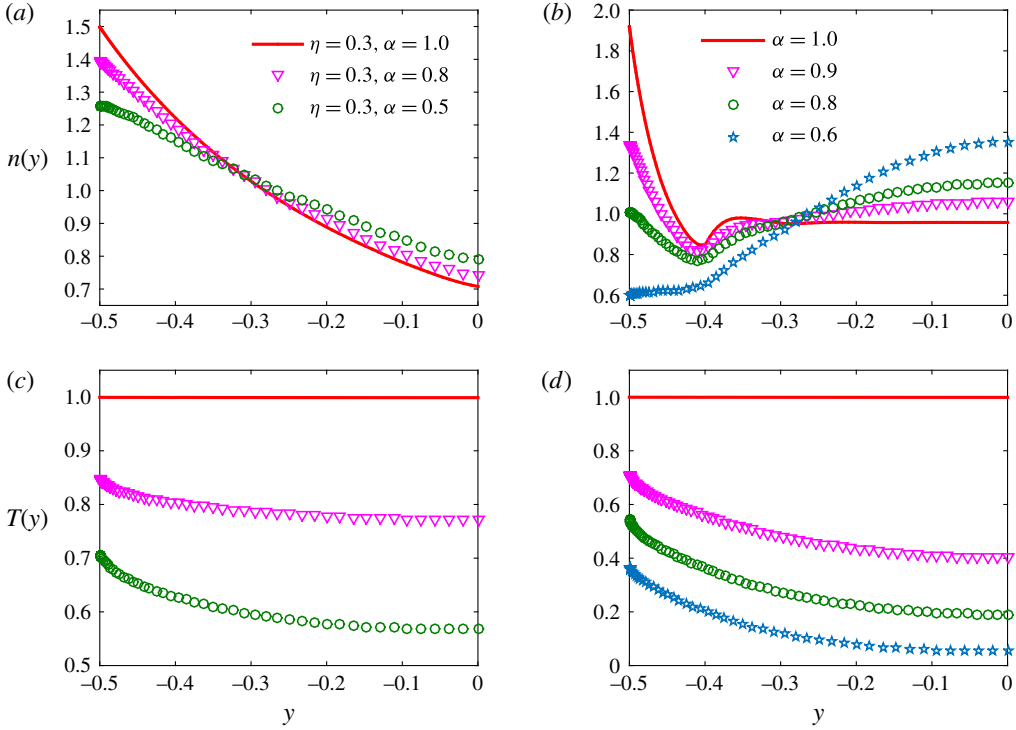


FIGURE 7. (Colour online) Normalized density (a,b) and temperature (c,d) profiles of the dense granular gas under tight confinements (a,c) $L/\sigma = 2$ and (b,d) $L/\sigma = 10$, for different values of the restitution coefficient. The normalized acceleration is $F = 0.0001$.

We first choose a small external acceleration ($F = 0.0001$). As the restitution coefficient α decreases, the gas temperature decreases monotonically from the wall to the channel centre, and the gas density near the wall (at the channel centre) decreases (increases); see figure 7. At large L/σ and small α , the gas concentrates in the channel centre and its density could even be larger than that near the wall. At fixed α , the decrease in the gas temperature gets larger when the solid fraction increases due to the increased number of dissipative collisions.

The anomalous velocity slip can be explained qualitatively using the shear viscosity (3.7), although the true viscosity is a function of the restitution coefficient (Garzó & Dufty 1999; Lutsko 2005). Taking into account the temperature variation across the channel, the slip velocity (3.10) may be extended to

$$V_x(y = \pm 1/2) \propto C \frac{\sqrt{\pi}}{2n(y = \pm 1/2)} \sqrt{\frac{T(y = \pm 1/2)}{T(y = 0)}}. \quad (3.11)$$

At fixed L/σ and fixed solid fraction η (i.e. the Knudsen number is fixed), both the gas density at the wall and the ratio of the bulk gas temperature to the near-wall gas temperature $T(0)/T(\pm 1/2)$ decreases with the restitution coefficient (see figure 7). Therefore, the velocity slip increases as the restitution coefficient decreases; see figure 8. On the other hand, for fixed L/σ and large values of α , the temperature ratio $T(0)/T(\pm 1/2)$ decreases but the near-wall gas density increases with the solid fraction, such that the slip velocity decreases with Kn , for example, when $L/\sigma = 10$ and $\alpha > 0.9$. When α is small, however, the decrease of $T(0)/T(\pm 1/2)$ with respect to the solid

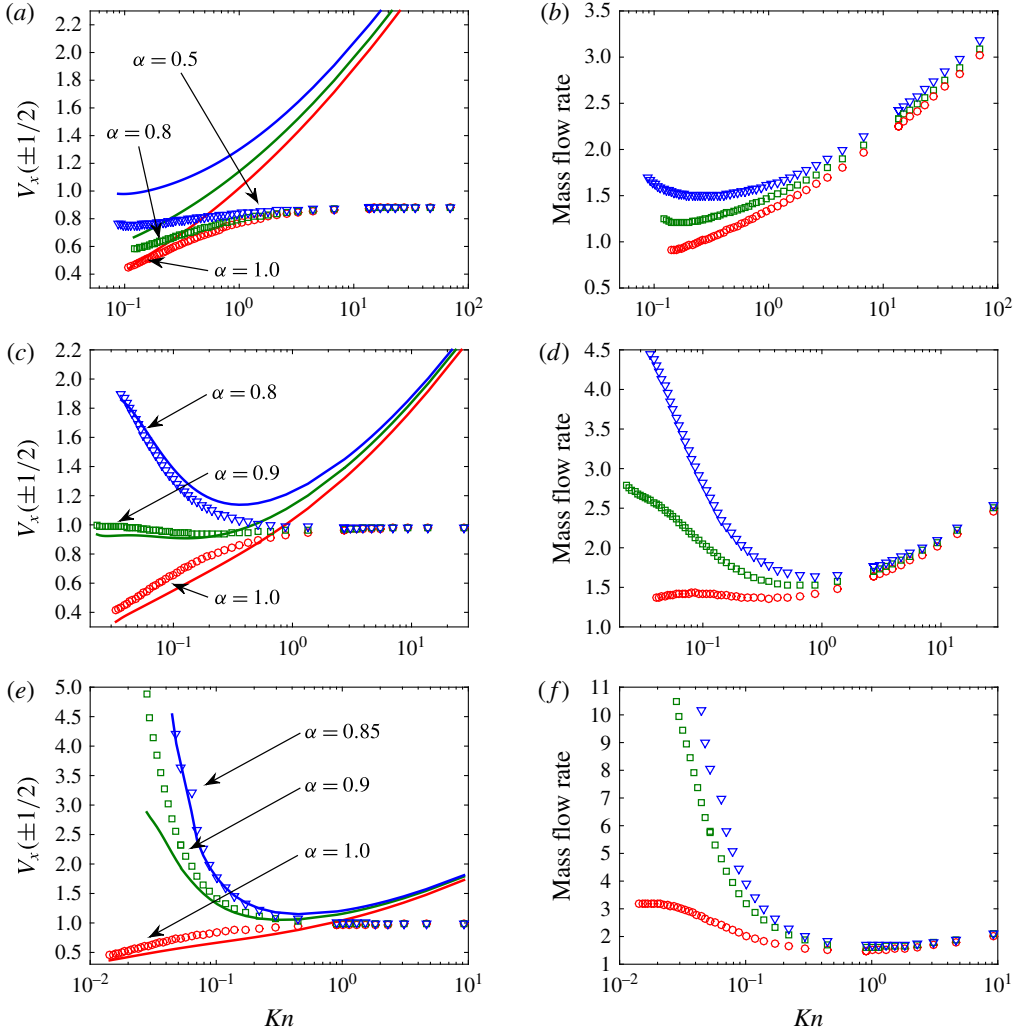


FIGURE 8. (Colour online) (a,c,e) The slip velocity and (b,d,f) the MFR of a dense granular gas for different values of the restitution coefficient α , when $L/\sigma = 2$ (a,b), 10 (c,d) and 30 (e,f), and the normalized acceleration is $F = 0.0001$. In (a,c,e) the lines are the velocity slip obtained from numerical solution of the generalized Enskog equation (2.2). Symbols are calculated from the numerical results according to (3.11).

fraction is rapid, and the slip velocity increases with decreasing Kn in the slip flow regime (this is the so-called anomalous velocity slip); for instance, see figure 8 for $\alpha = 0.8$ and $L/\sigma = 10$. For intermediate values of α , it is possible for the slip velocity to remain constant if the decrease of the temperature ratio $\sqrt{T(0)/T(\pm 1/2)}$ and the increase of the near-wall density cancel each other (see figure 8 for $\alpha = 0.9$ and $L/\sigma = 10$).

The variation of the MFR with the restitution coefficient is also shown in figure 8. In the free-molecular flow regime, the MFR is insensitive to the restitution coefficient since there are essentially no collisions between the hard discs. In the transitional and slip flow regimes, when Kn is fixed, the MFR increases as α decreases. One reason for this increase in MFR is that the velocity slip (and momentum slip) increases

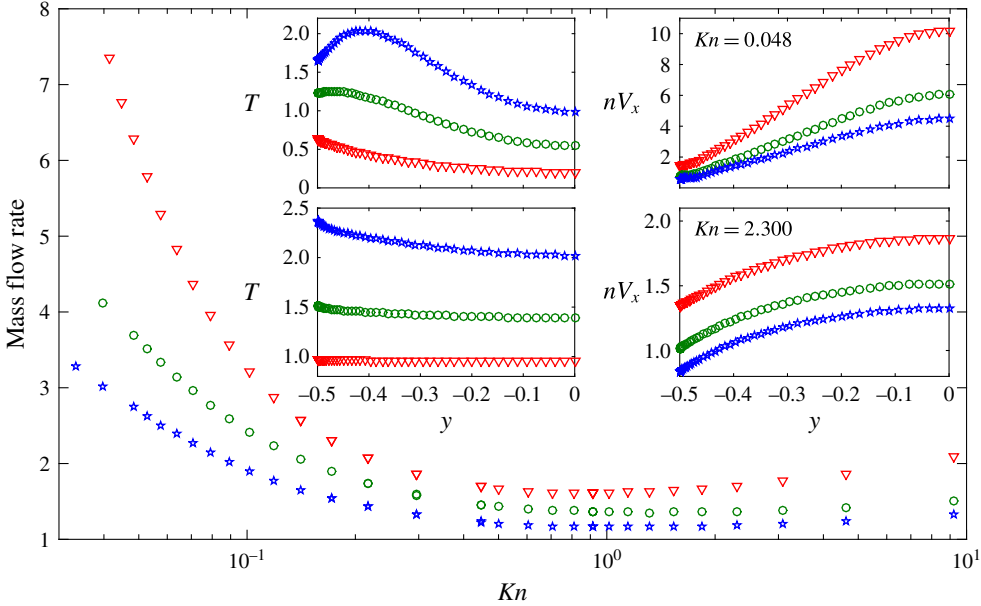


FIGURE 9. (Colour online) The influence of the external acceleration on the MFR at $L/\sigma = 30$, when the restitution coefficient is $\alpha = 0.9$. The normalized acceleration is $F = 0.0001$ (triangles), $F = 0.5$ (circles) and $F = 1$ (pentagrams). Inset: temperature and momentum profiles in the slip (first row) and transitional (second row) flow regimes.

when α decreases. Another reason is that the effective Knudsen number (roughly $\sqrt{T(y=0)}Kn_e$) decreases with α , which consequently makes the velocity profile steeper and increases the MFR. Interestingly, for $L/\sigma = 2$ the Knudsen minimum, which vanishes for elastic collisions, re-emerges when the collisions between hard discs are inelastic.

Finally, we consider the influence of large external accelerations (i.e. $F \sim 1$) on the MFR. For granular gases driven by a gravitational force, a large value of F is possible because of the large disc size and mass, and the small thermal velocity (Tij & Santos 2004). Figure 9 shows that the normalized MFR reduces with increasing external acceleration. This is consistent with results from Boltzmann-type kinetic equations (Aoki, Takata & Nakanishi 2002; Meng *et al.* 2013). Generally speaking, because of the viscous heating, a larger external acceleration results in a higher gas temperature and consequently a larger effective Knudsen number Kn_e . In the slip flow regime, a larger Kn_e has a flatter velocity profile and hence smaller MFR (see the first row in the inset of figure 9). Near the free-molecular flow regime, the slip velocity $U_x(y = \pm 1/2)$ is proportional to $\sqrt{T(y = \pm 1/2)}$, and since $\sqrt{T(y = \pm 1/2)}/F$ decreases as the normalized external acceleration F increases, the normalized velocity slip $V_x(y = \pm 1/2) = U_x(y = \pm 1/2)/F$ decreases as F increases (see the second row in the inset of figure 9), and so the MFR decreases because the normalized density profile is nearly unitary across the channel when Kn is large. Similar effects of the external force on the MFR are also observed at other values of L/σ and α .

4. Conclusions

Through both numerical solution of the generalized Enskog equation and analytical approaches, we have investigated the force-driven Poiseuille flow of a gas between two

parallel plates. The dilute-to-dense gas exhibited new flow physics due to the competition of three characteristic length scales: the mean free path, the channel width and the molecular diameter.

For elastic collisions in the hard-disc gas, we found the following. (i) In the slip flow regime, the normalized MFR becomes smaller as the confinement (i.e. L/σ) becomes tighter, for a fixed Knudsen number. In the limit of $L/\sigma \rightarrow \infty$, the MFR approaches that of the Boltzmann equation (in which the binary collisions are localized in space). When L/σ is fixed, the variation of the MFR with the Knudsen number is not monotonic. As the Knudsen number decreases from 0.1, the MFR first increases and then decreases; the maximum MFR occurs when the average solid fraction is approximately 0.3. We explained this exotic behaviour using the Navier–Stokes equation with a first-order velocity slip boundary condition. (ii) In the free-molecular flow regime, for a fixed Knudsen number, the MFR increases as L/σ is reduced, but in the limit $L/\sigma \rightarrow \infty$ the MFR is reduced to that of the Boltzmann equation. Our simple treatment of the average collision frequency accurately captures the influence of the tight wall confinement. (iii) In the transitional flow regime, for a fixed Knudsen number, the variation of the MFR with L/σ is not monotonic, and the minimum MFR is achieved at $L/\sigma \approx 2-3$.

When the collisions between the hard discs are inelastic, we found that the MFR increases as the restitution coefficient decreases due to the increase of the velocity slip and the decrease of the effective Knudsen number. We also proposed a simple formula to predict the anomalous velocity slip (which decreases as the Knudsen number increases). This simple formula and numerical solutions of the generalized Enskog equation also showed that the slip velocity could remain constant with varying Knudsen number at appropriate values of L/σ and the restitution coefficient. Finally, we showed that the normalized MFR reduces as the normalized external acceleration increases. Although we have only considered the diffuse boundary condition, the use of other momentum accommodation coefficients yield qualitatively the same results.

This research sheds new light on the influence of tight confinement on the mass flow rate of dense gases, and indicates that the MFR for Poiseuille flow obtained from the Boltzmann equation is not accurate for dense gases. For practical application to predicting the permeability of ultra-tight shale strata, more work needs to be done; for instance, to include the mean-field term so that a realistic equation of state for the shale gas is recovered, and to properly deal with the gas–wall interactions. Also, the inclusion of a mean-field term will enable us to study the flow dynamics of dense charged grains.

Acknowledgements

This work is financially supported by the UK's Engineering and Physical Sciences Research Council (EPSRC) under grants EP/M021475/1, EP/L00030X/1, EP/K038621/1, EP/I011927/1 and EP/N016602/1. H.L. gratefully acknowledges the financial support of the 'Thousand Talents Program' for Distinguished Young Scholars and the National Natural Science Foundation of China under grant no. 51506168.

REFERENCES

- ALAM, M., MAHAJAN, A. & SHIVANNA, D. 2015 On Knudsen-minimum effect and temperature bimodality in a dilute granular Poiseuille flow. *J. Fluid Mech.* **782**, 99–126.
- AOKI, K., TAKATA, S. & NAKANISHI, T. 2002 Poiseuille-type flow of a rarefied gas between two parallel plates driven by a uniform external force. *Phys. Rev. E* **65**, 026315.

- ARANSON, I. S. & TSIMRING, L. S. 2006 Patterns and collective behavior in granular media: theoretical concepts. *Rev. Mod. Phys.* **78**, 641–692.
- BARBANTE, P., FREZZOTTI, A. & GIBELLI, L. 2015 A kinetic theory description of liquid menisci at the microscale. *Kinet. Relat. Models* **8**, 235–254.
- BAUS, M. & COLOT, J. L. 1987 Thermodynamics and structure of a fluid of hard rods, disks, spheres, or hyperspheres from rescaled virial expansions. *Phys. Rev. A* **36**, 3912–3925.
- BOBYLEV, A. V., CARRILLO, J. A. & GAMBA, I. M. 2000 On some properties of kinetic and hydrodynamic equations for inelastic interactions. *J. Stat. Phys.* **98**, 743–773.
- BREY, J. J., DUFTY, J. W. & SANTOS, A. 1997 Dissipative dynamics for hard spheres. *J. Stat. Phys.* **87**, 1051–1066.
- BRILLIANTOV, N. & PÖSCHEL, T. 2004 *Kinetic Theory of Granular Gases*. Oxford University Press.
- CERCIGNANI, C. 1963 Plane Poiseuille flow and Knudsen minimum effect. In *Rarefied Gas Dynamics* (ed. J. A. Laurmann), vol. II, pp. 92–101.
- CERCIGNANI, C., LAMPIS, M. & LORENZANI, S. 2007 On the Reynolds equation for linearized models of the Boltzmann operator. *Transp. Theory Stat. Phys.* **36**, 257–280.
- CHAPMAN, S. & COWLING, T. G. 1970 *The Mathematical Theory of Non-Uniform Gases*. Cambridge University Press.
- DARABI, H., ETTEHAD, A., JAVADPOUR, F. & SEPEHRNOORI, K. 2012 Gas flow in ultra-tight shale strata. *J. Fluid Mech.* **710**, 641–658.
- ESTEBAN, M. J. & PERTHAME, B. 1991 On the modified Enskog equation for elastic and inelastic collisions. Models with spin. *Ann. Inst. Henri Poincaré* **8**, 289–308.
- FREZZOTTI, A. 1997 A particle scheme for the numerical solution of the Enskog equation. *Phys. Fluids* **9**, 1329–1335.
- FREZZOTTI, A. 1998 Molecular dynamics and Enskog theory calculation of shock profiles in a dense hard sphere gas. *Comput. Math. Applics.* **35**, 103–112.
- FREZZOTTI, A., GIBELLI, L. & LORENZANI, S. 2005 Mean field kinetic theory description of evaporation of a fluid into vacuum. *Phys. Fluids* **17**, 012102.
- FUKUI, S. & KANEKO, R. 1987 Analysis of ultra-thin gas film lubrication based on the linearized Boltzmann equation (influence of accommodation coefficient). *JSME Intl J.* **30**, 1660–1666.
- FUKUI, S. & KANEKO, R. 1990 A database for interpolation of Poiseuille flow rates for high Knudsen number lubrication problems. *J. Tribol.* **112**, 78–83.
- GALVIN, J. E., HRENYA, C. M. & WILDMAN, R. D. 2007 On the role of the Knudsen layer in rapid granular flows. *J. Fluid Mech.* **585**, 73–92.
- GARCIA-ROJO, R., LUDING, S. & BREY, J. J. 2006 Transport coefficients for dense hard-disk systems. *Phys. Rev. E* **74**, 061305.
- GARZÓ, V. & DUFTY, J. W. 1999 Dense fluid transport for inelastic hard spheres. *Phys. Rev. E* **59**, 5895–5911.
- GOLDSTEIN, A. & SHAPIRO, M. 1995 Mechanics of collisional motion of granular materials. Part 1. General hydrodynamic equations. *J. Fluid Mech.* **282**, 75–114.
- GRMELA, M. 1971 Kinetic equation approach to phase transitions. *J. Stat. Phys.* **3**, 347–364.
- GU, X. J. & EMERSON, D. R. 2009 A high-order moment approach for capturing non-equilibrium phenomena in the transition regime. *J. Fluid Mech.* **636**, 177–216.
- HADJICONSTANTINO, N. G. 2003 Comment on Cercignani's second-order slip coefficient. *Phys. Fluids* **15**, 2352–2354.
- HENDERSON, D. 1975 Simple equation of state for hard disks. *Mol. Phys.* **30**, 971–972.
- HOLT, J. K., PARK, H. G., WANG, Y., STADERMANN, M., ARTYUKHIN, A. B., GRIGORPOULOS, C. P., NOY, A. & BAKAJIN, O. 2006 Fast mass transport through sub-2-nanometer carbon nanotubes. *Science* **312**, 1034–1037.
- KARKHECK, J. & STELL, G. 1981 Mean field kinetic theories. *J. Chem. Phys.* **75**, 1475–1487.
- KARNIADAKIS, G., BESKOK, A. & ALURU, N. R. 2005 *Microflows and Manoflows: Fundamentals and Simulations*. Springer.
- KNUDSEN, M. 1909 Die Gesetze der Molekularströmung und der inneren Reibungsströmung der Gase durch Röhren. *Ann. Phys.* **333**, 75–130.

- KON, M., KOBAYASHI, K. & WATANABE, M. 2014 Method of determining kinetic boundary conditions in net evaporation/condensation. *Phys. Fluids* **26**, 072003.
- LUNATI, I. & LEE, S. H. 2014 A dual-tube model for gas dynamics in fractured nanoporous shale formations. *J. Fluid Mech.* **757**, 943–971.
- LUTSKO, J. F. 2005 Transport properties of dense dissipative hard-sphere fluids for arbitrary energy loss models. *Phys. Rev. E* **72**, 021306.
- MA, J., SANCHEZ, J. P., WU, K., COUPLES, G. D. & JIANG, Z. 2014 A pore network model for simulating non-ideal gas flow in micro- and nano-porous materials. *Fuel* **116**, 498–508.
- MEHMANI, A., PRODANOVIĆ, M. & JAVADPOUR, F. 2013 Multiscale, multiphysics network modeling of shale matrix gas flows. *Transp. Porous Med.* **88**, 377–390.
- MENG, J. P., WU, L., REESE, J. M. & ZHANG, Y. 2013 Assessment of the ellipsoidal-statistical Bhatnagar–Gross–Krook model for force-driven Poiseuille flows. *J. Comput. Phys.* **251**, 383–395.
- OHWADA, T., SONE, Y. & AOKI, K. 1989a Numerical analysis of the Poiseuille and thermal transpiration flows between two parallel plates on the basis of the Boltzmann equation for hard sphere molecules. *Phys. Fluids* **1**, 2042–2049.
- OHWADA, T., SONE, Y. & AOKI, K. 1989b Numerical analysis of the shear and thermal creep flows of a rarefied gas over a plane wall on the basis of the linearized Boltzmann equation for hard-sphere molecules. *Phys. Fluids A* **1**, 1588–1599.
- SANCHEZ, I. C. 1994 Virial coefficients and close-packing of hard spheres and discs. *J. Chem. Phys.* **101**, 7003–7006.
- TAKATA, S. & FUNAGANE, H. 2011 Poiseuille and thermal transpiration flows of a highly rarefied gas: over-concentration in the velocity distribution function. *J. Fluid Mech.* **669**, 242–259.
- TIJ, M. & SANTOS, A. 2004 Poiseuille flow in a heated granular gas. *J. Stat. Phys.* **117**, 901–928.
- WANG, Q., CHEN, X., JHA, A. & ROGERS, H. 2014 Natural gas from shale formation – the evolution, evidences and challenges of shale gas revolution in United States. *Renew. Sust. Energ. Rev.* **30**, 1–28.
- WU, L., ZHANG, Y. & REESE, J. M. 2015 Fast spectral solution of the generalized Enskog equation for dense gases. *J. Comput. Phys.* **303**, 66–79.